Int. J. Electrochem. Sci., 13 **(2018)** 1728 – 1743, doi: 10.20964/2018.02.08

International Journal of
ELECTROCHEMICAL
SCIENCE
www.electrochemsci.org

High–performance Activated Carbons Prepared by KOH Activation of Gulfweed for Supercapacitors

Shijie Li[1], *Kuihua Han*[1,*], *Pengchao Si*[2], *Jinxiao Li*[1], *Chunmei Lu*[1]

[1] School of Energy and Power Engineering, Shandong University, 250061 Jinan, PR China
[2] School of Material Science and Engineering, Shandong University, 250061 Jinan, PR China
[*]E–mail: hankh@163.com

Received: 26 September 2017 / *Accepted:* 24 November 2017 / *Published:* 28 December 2017

Activated carbons with huge specific surface area and developed pore structure are prepared by KOH activation of gulfweed. Six kinds of gulfweed–based activated carbons with different specific surface area are selected to investigate their electrochemical performance and the influence of specific surface area on the electrochemical performance. The electrochemical performance is investigated by galvanostatic charge–discharge and cyclic voltammetry test. The highest gravimetric capacitance is demonstrated by AC_{3155}, and the capacitance value reaches up to 395 F g^{-1} at the current density 0.05 A g^{-1} in 6 M KOH. Moreover, a slow fading of capacitance is observed as the current density increase. The capacitance retention is 92% after 10000 cycles at the current density 2.5 A g^{-1}. The gulfweed–based activated carbons demonstrate both excellent high rate capacitive performance and cycle performance.

Keywords: Gulfweed–based activated carbon; Specific surface area; Supercapacitors; Electrochemical performance.

1. INTRODUCTION

Because of the high specific surface area and developed pore structure, activated carbons are used in a wide range of applications, such as wastewater treatment [1], catalyst support [2], air purification [3], environmental remediation [4], and gas storage [5–7]. In the last ten years, activated carbons with abundant pore structures also have been highly demanded for energy storage devices, especially for supercapacitors [8–11]. Supercapacitors are considered to be one of the most promising energy storage devices, which have shown the bridging function of traditional dielectric capacitors and batteries/fuel cells in terms of energy and power densities with wide applications in mobile communication, solar and wind power, aerospace, national defense, computer power back–up, electric vehicles and power electronics [12–17]. Supercapacitors are mainly consist of electrode, electrolyte

and diaphragm, and the electrode materials in supercapacitors are the most important factor to define the ability of energy storage [18]. The electrode materials including carbon–based materials, metallic oxide materials and conducting polymer materials [19]. Activated carbons have become the most popular electrode materials due to its huge specific surface area, low price, relatively good electric conductivity, and excellent chemical stability in various electrolytes [20]. More than 80% of the commercial supercapacitors are fabricated based on porous carbon materials [21–23]. Thus, activated carbons with low price and excellent electrochemical performance are highly desired.

Almost all the carbon–containing materials can be treated as precursor to produce activated carbons [24]. Nowadays, most of the commercial activated carbons are prepared from fossil fuel–based precursors, such as coal and petroleum, which made them expensive and harmful to the environment [25]. While biomass–based materials have attracted an increasing interest in researches and applications due to their relatively low price, renewability, abundant supply, porous structure and environmentally friendly [26, 27]. In recent years, the use of biomass materials, such as coconut shell [28], corn [29], wheat straw [30], potato starch [31], rice husk [32], sunflower seed shell [33], white oak [34] and banana skin [35], as precursor to produce activated carbons for supercapacitors have gained much attention. The pore structures of activated carbons prepared from terrestrial plants is very dependent on the biomass structure, and the further optimization of the pore structure is limited to the traditional preparation method [36]. In addition, although some of the biomass–based activated carbons possess high specific surface area and reveal excellent electrochemical performance, the supply and collection are difficult for their biomass raw materials, such as agriculture straw and some fruit shell, which leads to that biomass–based activated carbons are difficult to be dominant commercial carbon materials. So it's meaningful and commercial attractive to find a kind of biomass–based activated carbon that possesses low cost, continuous raw material and shows excellent electrochemical performance.

In 2006, E. Raymundo–Pinero prepared activated carbons used for supercapacitors from a seaweed biopolymer, and it exhibited excellent electrochemical performance [37]. From then on, many researchers had turned their attention from terrestrial plants to seaweed plants. D.M. Kang [38] proposed a method for preparing the porous carbon with small mesopores from undaria pinnatifida, which showed excellent electrochemical performance. The porous carbon was used as electrode material for supercapacitors, even at relatively high charge–discharge rate, the gravimetric capacitance values of the porous carbon are 210 F g^{-1} and volumetric specific capacitance values are 120 F cm^{-3} in 1 M TEA BF_4/AN. In the previous study [39], activated carbons with developed pore structures were prepared by KOH activation of gulfweed. The obtained activated carbons possess not only high specific surface areas and large pore volumes, but also an appropriate pore width for transport of electrolyte ions. Which indicates the gulfweed–based activated carbon (GAC) a potential candidate for electrode materials for supercapacitors. As one of the most abundant seaweeds in China, gulfweed can be a continuous material for preparation of the activated carbon with relatively low price, moreover, the carbon yield in the activation process is considerate. Which results in the low cost of GAC and makes them promising for large–scale commercial applications.

In this paper, six kinds of GACs with stepwise distributed specific surface area and similar pore size distribution are selected to investigate their electrochemical performance, and the effect of the

specific surface area on electrochemical performance of the activated carbon are also investigated to determine the appropriate pore structure. The properties of activated carbons including functional groups, BET surface area, pore size distribution, microcrystalline structure and surface morphology were analyzed. Furthermore, the electrochemical test including cyclic voltammetry (CV) and galvanostatic charge–discharge (GCD) were carried out to investigate their electrochemical performance.

2. EXPERIMENTAL

2.1 Materials

Gulfweed is one of the widely distributed algae in Yellow Sea and is normally disposed as waste [40], which makes it possess relatively low economic value. In this paper, the gulfweed was obtained from Rongcheng Maoquan Aquatic Products Co., Ltd in Weihai City (Shandong, China). The aquatic products, including the gulfweed, of the company are mainly derived from Yellow Sea. The raw materials received were first thoroughly washed using tap water to remove the impurities and salinity and then dried at 120 °C for 48 h. After intensive drying, the gulfweed was grounded and sieved to get the gulfweed powder with a particle size under 180 μm. Ultimate analysis and proximate analysis of the gulfweed are shown in Table 1, which reveals that gulfweed not only has high carbon content but also has relatively higher nitrogen content compared with those terrestrial activated carbon precursors reported previously, such as wheat–straw [41] and rice straw [42] with nitrogen content of 0.44% and 0.65%, respectively. Generally, most of nitrogen functional groups have positive impact on electrochemical performance of activated carbons when they are applied to supercapacitors [43].

Table 1. Ultimate analysis and proximate analysis of the gulfweed

Ultimate analysis(wt.%)(ad)					Proximate analysis(wt.%)(ad)			
C	H	O	N	S	M	A	FC	V
41.41	5.42	34.98	3.39	1.67	2.40	10.73	14.93	71.94

Where M is the moisture, A is the ash, FC is the fixed carbon, V is the volatile.
Note: The proximate analysis was in accordance with the standard procedure of Chinese GB/T 28731–2012 codes. The ultimate analysis was carried out using an elemental analyzer (LecoTruSpec CHN) and sulfur analyzer (Leco S144DR).

2.2 Preparation of the GACs

The gulfweed powder was put into a tube furnace for carbonization at 600 °C under the protection of nitrogen for 2 h. Afterward, the carbonized products were immersed in saturated KOH solution according to certain impregnation ratio (the impregnation ratio, activation temperature and time were arranged in accordance with an $L_{16}(4^3)$ (four three–level factors) orthogonal design) at 80

°C for 2 h, the resulted mixture were put into a muffle furnace and heated to activation temperature with a heating rate of 5 °C min^{-1} at a certain activation time under a flow of nitrogen (2 NL min^{-1}). After natural cooling down to ambient temperature under nitrogen, the activation products were neutralized by 1 M HCl to pH 7, and then thoroughly washed with DI water to remove the ionic impurities. The resulted products were dried at 120 °C for 12 h and collected for the subsequent use. The obtained carbon samples were labeled as AC_x, where *x* represents the specific surface area.

2.3 Preparation of supercapacitors

The electrode slurry was prepared by mixing 80 wt.% of GAC, 10 wt.% PTFE emulsion (Polyflon, Daikin) and 10 wt.% of conductive graphite (KS6, TIMCAL) in appropriate amount of anhydrous ethanol. Then mixing them uniformly by ultrasonic dispersion treatment for 30 minutes. The slurry was evenly hand–painted onto the nickel foam with a diameter of 16 mm, the resulted carbon electrodes which contained about 10 mg activated materials were available. Thereafter, the electrodes were dried at 100 °C for 12 h in the vacuum drying oven to eliminate the superfluous anhydrous ethanol and then pressed under 12 MPa for 1 min by the use of hydraulic machine. Finally, a sandwich–type cell (CR2016 size) was assembled of two carbon–based electrodes separated by the diaphragm (NKK–MPF30AC–100). A 6 M KOH solution was adopted as the electrolyte to the supercapacitors.

2.4 Experimental techniques

N_2 adsorption–desorption measurements were carried out at 77 K by employing an ASAP 2020 (Micromeritics). Based on N_2 adsorption–desorption isotherms, the specific surface areas were calculated by using Brumauer–Emmett–Teller (BET) method, the pore size distributions were determined by Barrett–Joyner–Halanda (BJH) and Horvath–Kawazoe (HK) method. The X–ray diffraction (XRD, Rigaku D/MAX–2500PC, equipped with Cu radiation, λ = 5406 Å) was carried out to observe the graphitization structure. The Fourier transform infrared spectroscopy (FTIR) was carried out to determine the functional groups of the activated carbon. The spectra were exhibited over the range of 500–4500 cm^{-1} and 16 scan times were taken at a resolution of 4 cm^{-1}. The Supra 55 scanning electron microscope (SEM) (Carl Zeiss AG, Germany) was used for observing the surface morphology of the activated carbons. To investigate the electrochemical performance of activated carbons, the cyclic voltammetry (CV) and galvanostatic charge–discharge (GCD) test were measured on an electrochemical station (CS310H, CorrTest). The voltage window and scan rate were set to be 0–1 V and 5–200 mV s^{-1}, respectively. The GCD measurement was carried out at the current density ranging from 0.1–10 A g^{-1}. The gravimetric capacitances were calculated from the GCD curves of supercapacitors by employing the following formula [44]:

$$C_p = \frac{4i\Delta t}{m \propto \Delta V}$$

where C_p is the gravimetric capacitance (F g^{-1}), i is the discharge current (A), Δt is the discharging time (s), m is the mass of two electrodes (g), $\propto$ is the mass fraction of active materials in the electrode (wt%), ΔV is the potential difference in the discharging process (V).

3. RESULTS AND DISCUSSION

3.1 Pore structure of the GACs

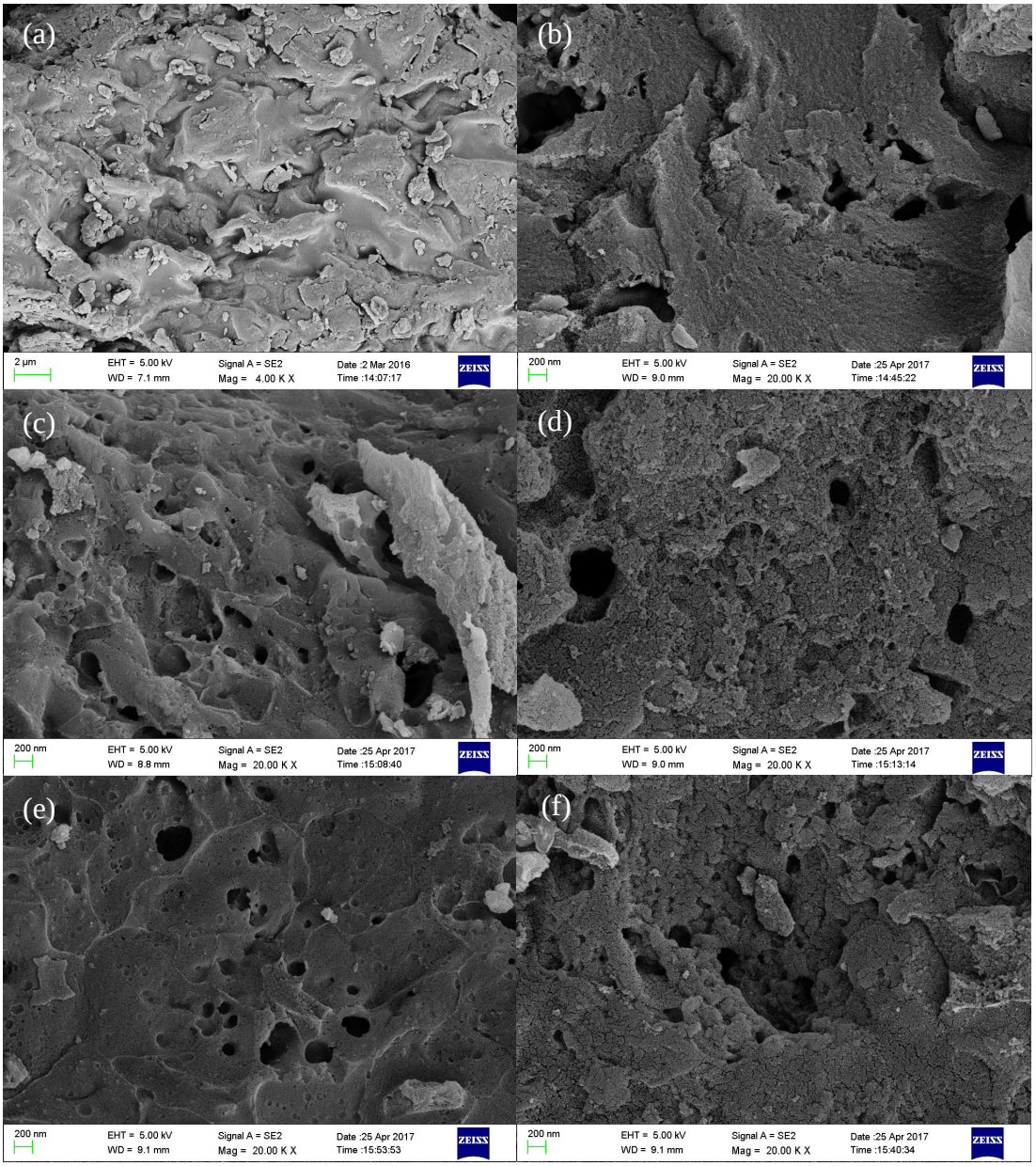

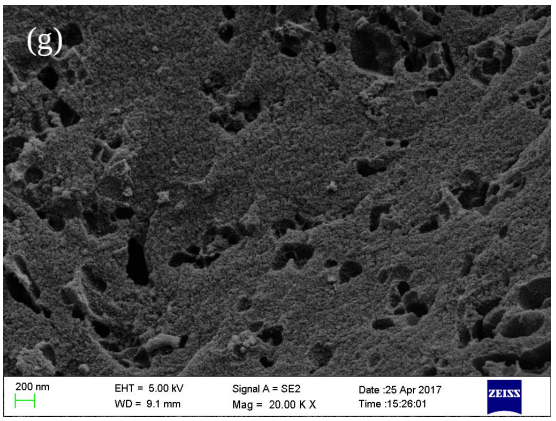

Figure 1. SEM images of the gulfweed and GACs

It is generally recognized that the specific surface area and pore structure play an important role for electrochemical performance of activated carbons [45]. In practical applications, the activated carbons with large specific surface area and abundant pore structure are usually considered as preferable electrode materials [46, 47]. The SEM images of the gulfweed and GACs are presented in Fig. 1 at magnification of ×20000. Fig. 1(a)–(g) show the SEM images of the gulfweed, AC_{2227}, AC_{2422}, AC_{2674}, AC_{2862}, AC_{3155} and AC_{3362}, respectively. The significant changes between the surface morphology of gulfweed and GACs are observed. The structure of gulfweed material is smooth and tight, and has barely pores available on the surface. The structures of the GACs are loose and porous, and a large amount of pores were observed on the surface of the activated carbons.

The pore size distribution also significantly affects the electrochemical performance of activated carbon. An appropriate pore size distribution can greatly enhance the utilization of specific surface area [48]. In carbon materials used in supercapacitors, ion–accessible micropores (< 2 nm) are primarily responsible for the capacitance properties [38], the increase of effective micropore surface area can significantly improve their capacitance [49]. Mesopores (2–50 nm) and macropores (> 50 nm) are associated with high–rate capacitive performance by providing low resistance ion transport channels to the interior surface [50, 51]. Hence, hierarchically activated carbons with large specific surface area and appropriate pore size distribution are highly desired for supercapacitors. The detailed textural properties of the GACs are shown in Table 2 [39]. All the GACs have huge specific surface areas of over 2200 $m^2\ g^{-1}$. The N_2 adsorption–desorption isotherms and pore size distributions of the GACs are shown in Fig. 2. The N_2 adsorption–desorption isotherms of GACs show the characteristics of type IV. The steep increase of isotherms at low relative pressure (P/P_0 <0.1) indicates the existence of a large amount of micropores [52].

Besides, obvious hysteresis loops are observed from all isotherms in the relative pressure 0.4–1, which is related to the capillary condensation in mesopores, indicates the existence of mesopores in activated carbons [53, 54]. It could be clearly seen from the pore size distributions (Fig. 2(b)) that GACs possess a large amount of micropores in the range of 0.4–0.8 nm and some mesopores in the range of 2–4 nm. It has been proved that pores with diameter 0.4–1 nm and 2–4 nm contribute a lot to the capacitance and rate performance, respectively [38].

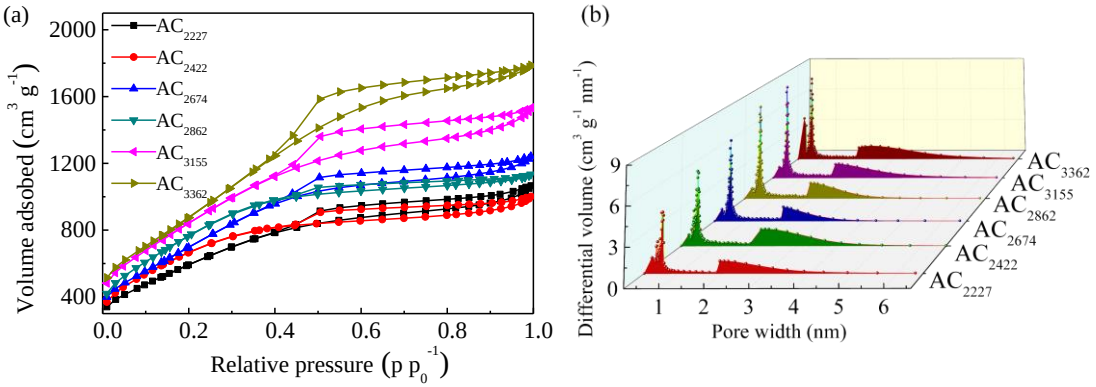

Figure 2. (a) N_2 adsorption–desorption isotherms of GACs. (b) Pore size distributions of GACs.

According to the nitrogen adsorption data, most of the pores of the GACs are in the range which allows an optimized electrosorption and transport of ions [55–58]. Therefore, we attempt to investigate the electrochemical performance of these activated carbons, and expect to find a kind of activated carbon with both low price and excellent electrochemical performance.

Table 2. Textural properties of the GACs

Sample	S_{BET} (m^2 g^{-1})	V_{total} (cm^3 g^{-1})	V_{micro}(cm^3 g^{-1})	V_{mes} (cm^3 g^{-1})	L_o (nm)
AC_{2227}	2227	1.65	0.83	0.82	2.96
AC_{2422}	2422	1.55	0.75	0.8	2.56
AC_{2674}	2674	1.92	1.02	0.9	2.87
AC_{2862}	2862	1.75	0.87	0.88	2.45
AC_{3155}	3155	2.37	1.32	1.05	3.01
AC_{3362}	3362	2.77	1.29	1.48	3.29

3.2 Electrochemical performance

In order to investigate the electrochemical performance, two–electrodes symmetrical supercapacitors were fabricated and measured using best–practice methods with 6 M KOH as an electrolyte. Cyclic voltammogram (CV) is one of the most common characterization methods to investigate the electrochemical performance of carbon materials in supercapacitors [59]. Fig. 3(a) shows the CV curves of six GACs at a scan rate of 10 mV s^{-1}, the CV curves of all activated carbons show symmetric rectangular shapes, implying an ideal electrical double–layer effect of all the tested supercapacitors. Besides, inexistence of any redox peaks at CV curves is observed, implying the absence of pseudocapacitance. Among these GACs, the largest current density is demonstrated by AC_{3155} and its CV properties at higher scan rate were further investigated. It can be clearly seen from the Fig. 3(b) that the CV curves of AC_{3155} have always been symmetric rectangular shapes as the scan rate increased from 20 to 100 mV s^{-1}, implying that the AC_{3155} electrodes possess relatively strong ion transport ability, which results in the quick charge propagation in AC_{3155} electrodes [38].

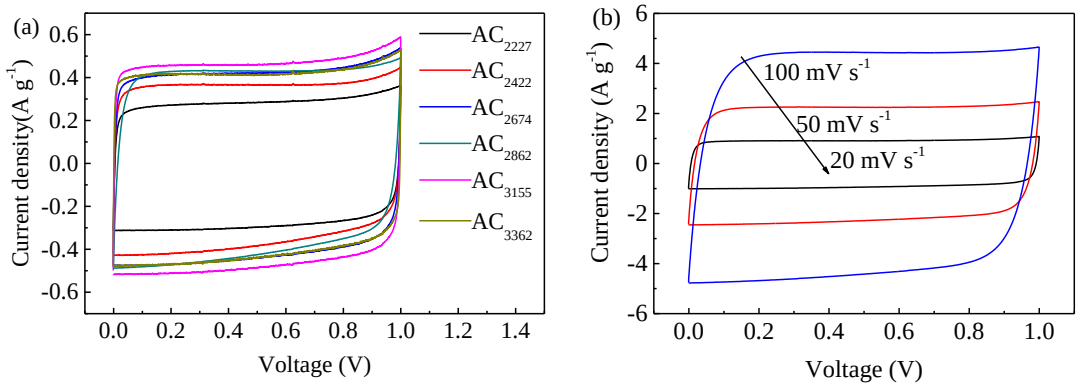

Figure 3. (a) CV curves of six activated carbons at a scan rate of 10 mV s^{-1}. (b) CV curves of AC_{3155} at different scan rate.

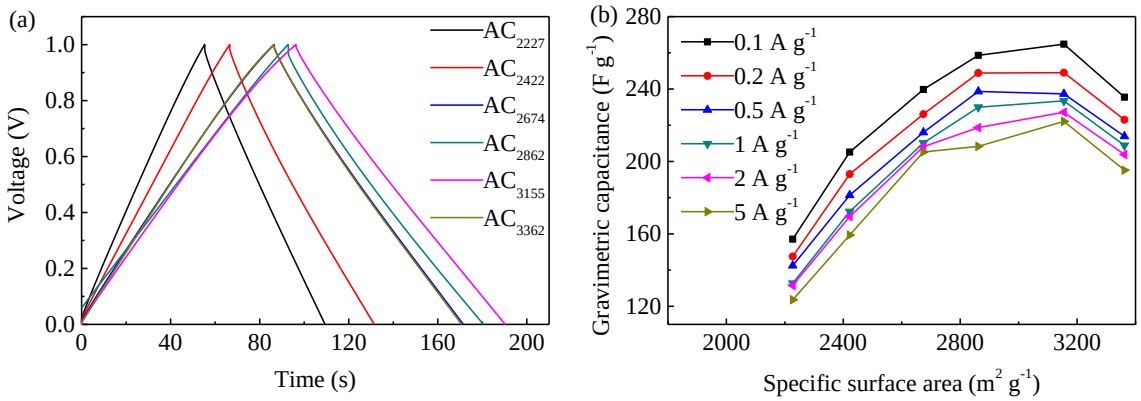

Figure 4. (a) GCD curves of six activated carbons at a current density of 0.5 A g^{-1}. (b) The relationship between specific surface area and gravimetric capacitance

Table 3. The capacitance values at 0.1 A g^{-1} of biomass-based activated carbon

No	Materials	Activation agent	Electrolyte	S_{BET} (m^2 g^{-1})	Capacitance (F g^{-1})	Reference
1	Coconut shell	KOH	KOH	3436	368	[28]
2	Corn	KOH	KOH	3199	257	[29]
3	Wheat straw	KOH	$MeEt_3NBF_4$	2316	251	[30]
4	Potato starch	KOH	KOH	2342	335	[31]
5	Rice husk	NaOH	KOH	3969	368	[32]
6	Sunflower seed shell	KOH	KOH	2509	311	[33]
7	Gulfweed	KOH	KOH	3155	265	This work

The galvanostatic charge–discharge (GCD) curves of six GACs at the current density of 0.5 A g^{-1} are shown in Fig. 4(a). The GCD testing yields symmetric triangle curves of all the GAC–based electrodes, which indicates that the tested supercapacitors possess relatively small equivalent series resistance and high charge–discharge efficiency. Capacitance is one of the most important performance index of supercapacitors, high capacitance is always the target of the researchers in this field. In this study, the gravimetric capacitance values of GACs are calculated from the GCD discharge data. The highest capacitance is exhibited by AC_{3155}, and its gravimetric capacitance values are 265, 249, 237, 233, 227, 225 and 222 F g^{-1} at a current density of 0.1, 0.2, 0.5, 1, 2, 2.5 and 5 A g^{-1}, respectively. These capacitance values are almost as much as those of some terrestrial biomass–based activated carbons, such as corn [29] and wheat straw [30]. The capacitance values at 0.1 A g^{-1} of biomass-based activated carbon are shown in Table 3. In addition, the gravimetric capacitance value of AC_{3155} can reach up to 395 F g^{-1} when the supercapacitors tested at a relatively small current density of 0.05 A g^{-1}.

At the current density of 0.5 A g^{-1}, the rank of the gravimetric capacitance values is AC_{3155} >AC_{2862} >AC_{2674} >AC_{3362} >AC_{2422} >AC_{2227}, when the specific surface area increases from 2227 m^2 g^{-1} to 3155 m^2 g^{-1}, the gravimetric capacitance values increase gradually in good agreement with specific surface area, while the opposite situation is observed when the specific surface area keeps increasing to 3362 m^2 g^{-1}, indicating that the gravimetric capacitance is not fully in accordance with the specific surface area. For further study, the relationship between specific surface area and gravimetric capacitance is investigated at different current density (0.1–5 A g^{-1}), the similar tendency at various current density is observed as shown in Fig. 4(b). When the specific surface area increases from 2227 m^2 g^{-1} to 2862 m^2 g^{-1}, the relationship between specific surface area and gravimetric capacitance value presents good linearity. This is because the AC_{2227}, AC_{2422}, AC_{2674} and AC_{2862} possess similar pore size distribution, with the increase of specific surface area, the effective micropore specific surface area and ion transport channels of GACs increase linearly, which results in the generation of more double layer capacitance.

With the continued increase of the specific surface area, the linearity relationship disappears and a negligible increase is observed at the specific surface area 3155 m^2 g^{-1}. Reasons for this phenomenon are multi–aspect, except for the pore size distribution, the microcrystalline structure and surface functional groups of activated carbon also affect its capacitance property [45]. The XRD patterns of the GAC samples are shown in Fig. 5. The XRD patterns for AC_{2227}, AC_{2422}, AC_{2674} and AC_{2862} demonstrate two sharp diffraction peaks at 2θ=23°and 44°, which corresponding to (002) and (100) diffractions for carbon. This indicates that these activated carbon samples have a certain graphite microcrystalline structure [60]. Activated carbons with high specific surface area usually have a relatively poor electrical conductivity due to their abundant pore structures, the existence of graphite microcrystalline can greatly improve their electrical conductivity, which resulted for the improvement of their electrochemical performance. With the increase of the specific surface area, the two sharp diffraction peaks are disappeared in AC_{3155} and AC_{3362}, indicating that the graphite microcrystalline structure in the carbon materials has been destroyed in the chemical etching process.

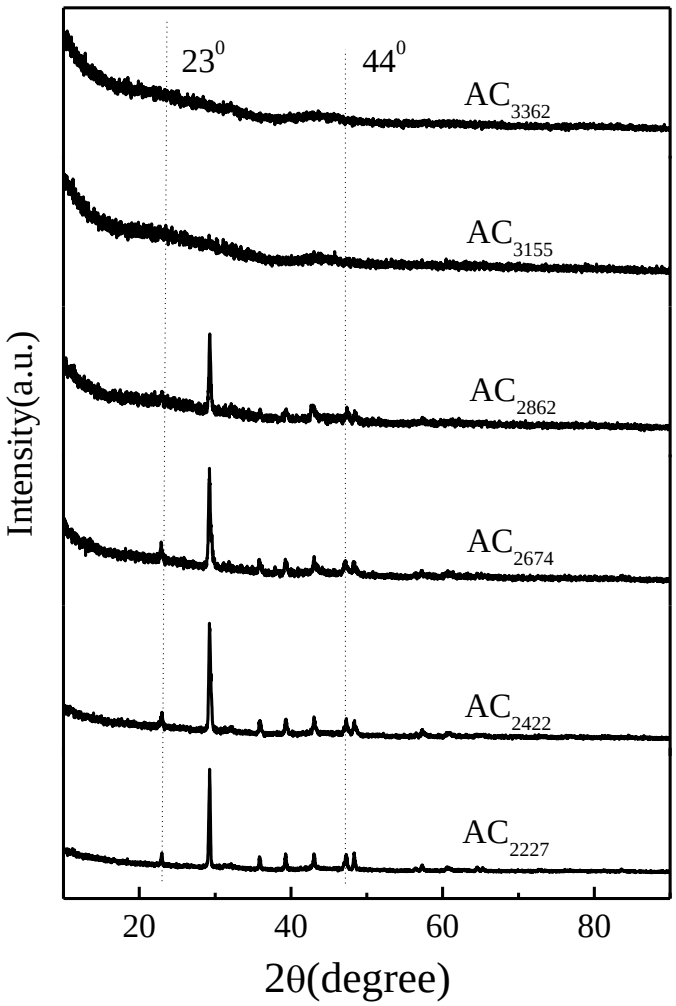

Figure 5. XRD patterns of the activated carbon samples.

The surface functional groups are associated with the electrochemical performance of the carbon materials by influencing their wettability, polarity and stability [61–65]. In addition, the existence of some surface functional groups can improve the capacitance by generating pseudocapacitance [66]. The FTIR spectra of the GACs are shown in Fig. 6. The surface functional groups of the carbon samples are similar but a little difference, the peak around 710 cm^{-1} in the AC_{2227}, AC_{2422}, AC_{2674}, AC_{2862} spectra are assigned to N–H bonding vibration peak [67]. The existence of surface functional group N–H can significantly improve the hydrophilia and wettability of the activated carbon, which leads to the increased utilization rate of specific surface area and greatly improvement for the electrochemical performance of the supercapacitors [68]. Compared to AC_{2862}, the negligible capacitance increase of AC_{3155} results from the combined influences of specific surface area, pore size distribution, graphite microcrystalline structure and surface functional groups.

A deeply decrease of gravimetric capacitance is occurred when the specific surface area increases from 3155 m^2 g^{-1} to 3362 m^2 g^{-1}. From the XRD and FT–IR analysis, AC_{3155} and AC_{3362} have extremely similar microcrystalline structure and surface functional groups. So the decrease of gravimetric capacitance mainly results from the difference of pore size distributions.

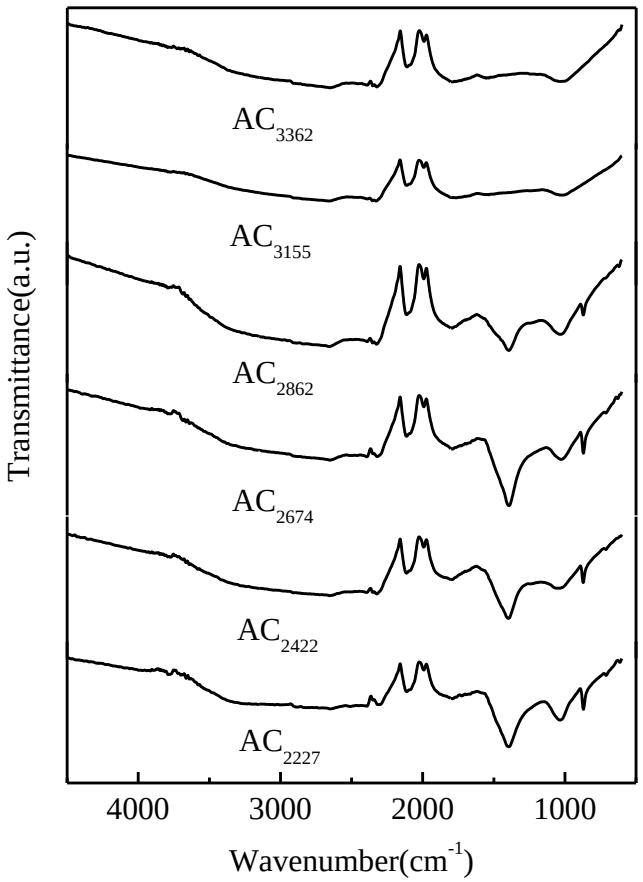

Figure 6. FT–IR spectra of the activated carbon samples.

It could be seen from the Fig. 2 that AC_{3155} and AC_{3362} possess a large amount of micropores in the range of 0.4–0.8 nm, while AC_{3362} presents more small micropores with a diameter of 0.4–0.5 nm but fewer micropores with a diameter of 0.5–0.8 nm when compared with the AC_{3155}, indicating that the increase of specific surface area mainly comes from the increase of small micropores with a diameter of 0.4–0.5 nm. Which demonstrates that the micropores with a diameter of 0.5–0.8 nm are more beneficial to the formation of double layer capacitance than the micropores with a diameter of 0.4–0.5 nm. This is the reason why AC_{3362} possess large specific surface area but smaller gravimetric capacitance than AC_{3155}.

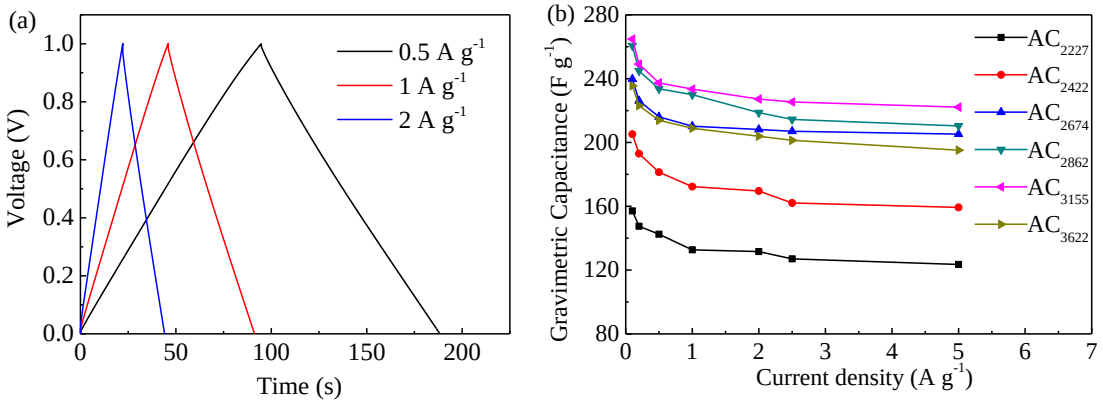

Figure 7. (a) GCD curves of AC_{3155} at the different current density. (b) The gravimetric capacitance values of six activated carbons at different current density.

Rate performance of the activated carbons is an important index for their high power applications. The GCD curves of AC_{3155} at the different current density are shown in Fig. 7(a). It can be seen that the curves can always show the typical isosceles triangle shapes when the current density increases from 0.5 to 2 A g^{-1}. Even at a large current density of 2 A g^{-1}, a negligible voltage difference was observed at the beginning of discharge process, which demonstrates the low equivalent series resistance and excellent rate performance of the AC_{3155}.

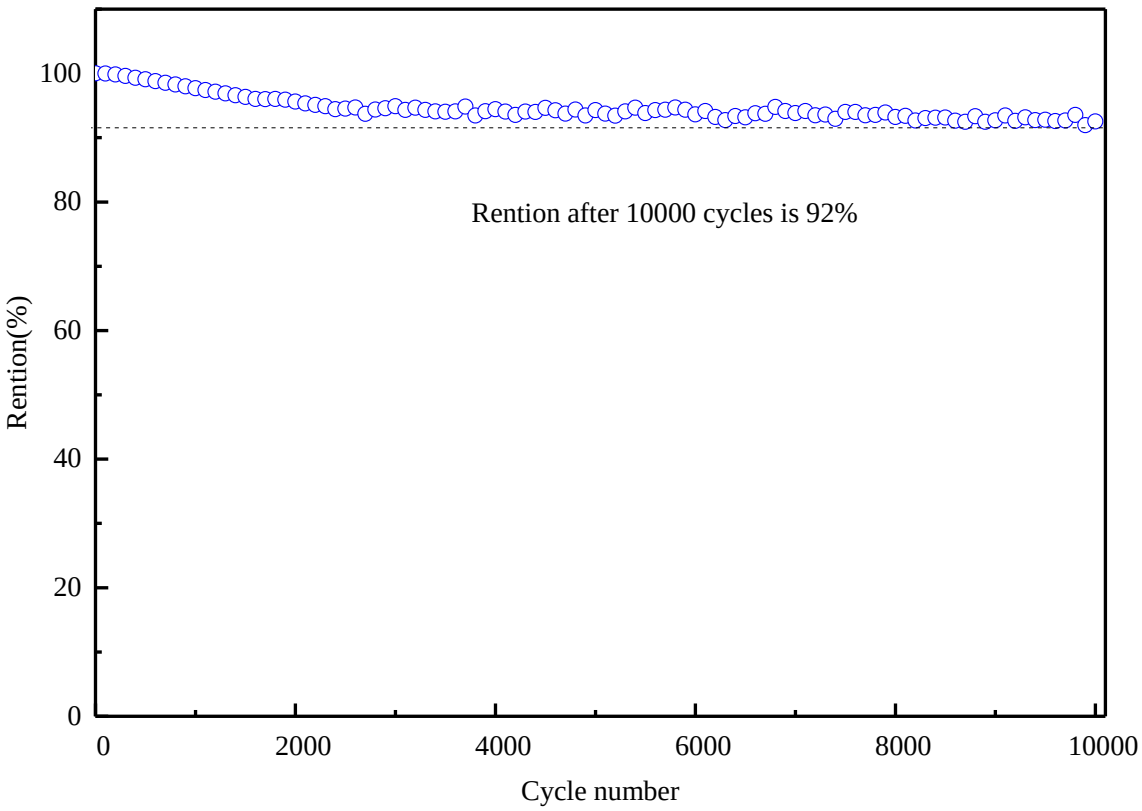

Figure 8. Cycle performance of the AC_{3155} in 6 M KOH electrolyte at a current density of 2.5 A g^{-1}

To investigate the detailed rate performance, the gravimetric capacitance values of the GACs were calculated from the GCD discharge data at the current density of 0.1, 0.2, 0.5, 1, 2, 2.5 and 5 A g^{-1}. From the Fig. 7(b), the gravimetric capacitance values of all the GACs show slow fading as the current density increases. When the current density increases from 0.1 to 5 A g^{-1}, the gravimetric capacitance retention rates of AC_{2227}, AC_{2422}, AC_{2674}, AC_{2862}, AC_{3155} and AC_{3362} are 83.8%, 77.6%, 85.5%, 74%, 83.9% and 82.9%, respectively. Especially when the current density exceeds 1 A g^{-1}, the capacitance retention rates of AC_{2227}, AC_{2422}, AC_{2674}, AC_{2862}, AC_{3155} and AC_{3362} reaches up to 99.2%, 92.4%, 97.5%, 90.6%, 95.1% and 93.4%, respectively, which indicates that the GACs possess excellent rate performance even at high current density. The supercapacitors can still retain high capacitance when work at relatively large charge current density, which result in not only a high capacitance but also a short charging time. This reveals that the GACs can still demonstrate excellent electrochemical performance in high power application, which makes the GACs more suitable for the practical applications.

Like some other aspects of electrochemical performance, cycle performance also plays a vital role for the service life of supercapacitors by determining their cycling stability. Cycling performance of AC_{3155} was carried out at a current density of 2.5 A g^{-1} for 10 000 cycles in 6 M KOH. It can be seen from the Fig. 8 that the AC_{3155} shows excellent cycle performance. The gravimetric capacitance has relatively high retention from its initial value, the capacitance retention after 10000 cycles is as high as 92%, especially after 3000 cycles, the specific capacitance fades at a negligible rate, that because since the charge storage in AC_{3155} was dominated by the pure electric double layer energy storage, the charge–discharge process in the electrodes is almost completely reversible [38].

4. CONCLUSION

In this paper, gulfweed is selected as precursor materials to produce the activated carbons, all the carbon products prepared at different experimental conditions possess huge specific surface areas over 2200 m^2 g^{-1} and large pore volumes, the biggest specific surface area and pore volume reach up to 3362 m^2 g^{-1} and 2.77 cm^3 g^{-1}, respectively. The electrochemical performances of AC_{2227}, AC_{2422}, AC_{2674}, AC_{2862}, AC_{3155} and AC_{3362} are investigated by cyclic voltammetry and galvanostatic charge–discharge measurements. All the activated carbon samples show relatively better electrochemical performance, especially AC_{3155}, the gravimetric capacitance value of AC_{3155} reaches up to 395 F g^{-1} at the current density 0.05 A g^{-1}. The gravimetric capacitances of six activated carbons demonstrates slow fading as the current density increases, which indicates that they possess excellent rate performance at high current density. After 10,000 cycles at the current density of 2.5 A g^{-1}, the gravimetric capacitance has small decayed from its initial value (the retention is 92%), indicating that AC_{3155} displays excellent cycle stability at a relatively high current density. The experimental results demonstrate that the relationship between specific surface area and gravimetric capacitance value present good linearity when the carbon materials possess same pore size distribution, microcrystalline structure and surface functional groups. Moreover, the micropores with a diameter of 0.5–0.8 nm are

more beneficial to the formation of double layer capacitance than the micropores with a diameter of 0.4–0.5 nm in KOH electrolyte.

ACKNOWLEDGEMENTS
This study was supported by the Natural Science Foundation of Shandong, China (ZR2017MEE010), the Fundamental Research Funds of Shandong University (2016JC005), and the Science and Technology Development Plan Project of Shandong Province (2016GGX104005).

References

1. V. Kårelid, G. Larsson and B. Björlenius, *J. Environ. Manage*., 193 (2017) 491.
2. M.A. Patel, F.X. Luo, K. Savaram, P. Kucheryavy, Q.Q. Xie, C. Flach, R. Mendelsohn, E. Garfunkel, J.V. Lockard and H.X. He, *Carbon*, 114 (2017) 383.
3. A.H. Mamaghani, F. Haghighat and C.S. Lee, *Appl. Catal*., B 203 (2017) 247.
4. A. Gomis–Berenguer, L.F. Velasco, I. Velo–Gala and C.O. Ania, *J. Colloid Interface Sci*., 490 (2017) 879.
5. A. Gundogdu, C. Duran, H.B. Senturk, M. Soylak, D. Ozdes, H. Serencam and M. Imamoglu, *J. Chem. Eng. Data*, 57 (2012) 2733.
6. I. Martin–Gullon, J.P. Marco–Lozar, D. Cazorla–Amorós and A. Linares–Solano, *Carbon*, 42 (2004) 1339.
7. S. Biloé, V. Goetz and A. Guillot, *Carbon*, 40 (2002) 1295.
8. M.A. Habila, Z.A. Alothman, S.A. Al–Tamrah, A.A. Ghafar and M. Soylak, *J. Ind. and Eng. Chem*., 32 (2015) 336.
9. M. Soylak, *Fresenius Environ. Bull*., 7 (1998) 383.
10. H. Oda and Y. Nakagawa, *Carbon*, 41 (2003) 1037.
11. J. Yi, Q. Yan, C.T. Wu, Y.X. Zeng, Y.Q. Wu, X.H. Lu and Y.X. Tong, *J. Power sources*, 351 (2017) 130.
12. B.H. Patil, A.D. Jagadale and C.D. Lokhande, *Synthetic Met*, 162 (2012) 1400.
13. J.R. Miller and P. Simon, *Science*, 321 (2008) 651.
14. A. Lewandowski and M. Galinski, *J. Power sources*, 173 (2007) 822.
15. O. Bohlen, J. Kowal and D.U. Sauer, *J. Power sources*, 172 (2007) 468.
16. Y.S. Yun, S.Y. Cho, J.Y. Shim, B.H. Kim, S.J. Chang, S.J. Baek, Y.S. Huh, Y.S. Tak, Y.W. Park, S.J. Park and H.J. Jin, *Adv. Mater*, 25 (2013) 1993.
17. L.F. Chen, X.D. Zhang, H.W. Liang, M.G. Kong, Q.F. Guan, P. Chen, Z.Y. Wu and S.H. Yu, *ACS Nano*, 6 (2012) 7092.
18. C. Jackson, M. Shahsahebi, T. Wedlake and C.A. Dubard, *Energ Environ Sci*, 6 (2013) 2465.
19. X.C. Dong, J.X. Wang, J. Wang, M.B. Chan–Park, X.G. Li, L.H. Wang, W. Huang and P. Chen, *Mater. Chem. Phys*., 137 (2012) 576.
20. Y. Xiao, C. Long, M.T. Zheng, H.W. Dong, B.F. Lei, H.R. Zhang and Y.L. Liu, *Chin. Chem. Lett*., 25 (2014) 865.
21. P. Simon and Y. Gogotsi, *Acc. Chem. Res*, 46 (2013) 1094.
22. Y.P. Zhai, Y.Q. Dou, D.Y. Zhao, P.F. Fulvio, R.T. Mayes and S. Dai, *Adv. Mater*., 23 (2011) 4828.
23. W. Zhang, Y.H. Yao and L.J. Gao, *Chin. Chem. Lett*., 23 (2012) 623.
24. P. Kleszyk, P. Ratajczak, P. Skowron, J. Jagiello, Q. Abbas, E. Frąckowiak and F. Béguin, *Carbon*, 81 (2015) 148.

25. A.M. Abioye and F.N. Ani, *Sust. Energ. Rev*., 52 (2015) 1282.
26. R. Farma, M. Deraman, A. Awitdrus, I.A. Talib, E. Taer, N.H. Basri, J.G. Manjunatha, M.M. Ishak, B.N.M. Dollah and S.A. Hashmi, *Bioresour Technol*, 132 (2013) 254.
27. G. Wang, Y. Ling, F. Qian, X. Yang, X.X. Liu and Y. Li, *J. Power Sources*, 196 (2011) 5209.
28. K. Jurewicz and K, Babeł, *Energy Fuel*, 24 (2010) 3429.
29. M.S. Balathanigaimani, W.G. Shim, M.J. Lee, C. Kim, J.W. Lee and H. Moon, *Electrochem Commun*, 10 (2008) 868.
30. X.L. Li, C.L. Han, X.Y. Chen and C.W. Shi, *Microporous Mesoporous Mater*, 131 (2010) 303.
31. S. Zhao, C.Y. Wang, M.M. Chen, J. Wang and Z.Q. Shi, *J Phys Chem Solids*, 70 (2009) 1256.
32. H.B. Chen, H.B. Wang, L.F. Yang and H.G. Fu, *Int. J. Electrochem. Sci*., 7 (2012) 4889.
33. X. Li, W. Xing, S.P. Zhuo, J. Zhou, F. Li, S.Z. Qiao and G.Q. Lu, *Bioresour. Technol*., 102 (2011) 1118.
34. M. Jagtoyen and F. Derbyshire, *Carbon*, 36 (1998) 1085.
35. Y. Lv, L. Gan, M. Liu, W. Xiong, Z. Xu, D. Zhu and D.S. Wright, *J. Power Sources*, 209 (2012) 152.
36. A.M. Abioye and F.N. Ani, *Sust. Energ. Rev*., 52 (2015) 1282.
37. E. Raymundo–Pinero, F. Leroux and F. Beguin, *Adv. Mater*., 18 (2006) 1877.
38. D.M. Kang, Q.L. Liu, J.J. Gu, Y.S. Su, W. Zhang and D. Zhang, *ACS Nano*, 9 (2015) 11225.
39. S.J. Li, K.H. Han, J.X. Li, M. Li and C.M. Lu, *Microporous Mesoporous Mater*, 243 (2017) 291.
40. L. Wei, T. Shan and S. Yun, *Fuel*, 160 (2015) 35.
41. H. Haykırı–Açma, *Energy Convers. Manage*., 44 (2003) 155.
42. L. Deng, T. Zhang and D. Che, *Fuel Process. Technol*., 106 (2013) 712.
43. Y.R. Nian and H. Teng, *J. Eiectroanal. Chem*., 540 (2003) 119.
44. D. Qu and H. Shi, *J. Power sources*, 74 (1998) 99.
45. Z.H. Wen and J.H. Li, *J. Mater. Chem*., 19 (2009) 8707.
46. A.G. Pandolfo and A.F. Hollenkamp, *J. Power Sources*, 157 (2006) 11.
47. L.L. Zhang and X.S. Zhao, *Chem. Soc. Rev*, 38 (2009) 2520.
48. Z.Y. Li, M.S. Akhtar, D.H. Kwak and O.B. Yang, *Appl. Surf. Sci*, 404 (2017) 88.
49. E. Raymundo–Piñero, K. Kierzek, J. Machnikowski and F. Béguin, *Carbon*, 44 (2006) 2498.
50. Z.S. Wu, Y. Sun, Y.Z. Tan, S. Yang, X. Feng and K. Müllen, *J. Am. Chem. Soc*., 134 (2012) 19532.
51. D.W. Wang, F. Li, M. Liu, G.Q. Lu and H.M. Cheng, *Angew. Chem.–Int. Edit*., 47 (2008) 379.
52. P. Kleszyk, P. Ratajczak, P. Skowron, J. Jagiello, Q. Abbas, E. Frąckowiak and F. Béguin, *Carbon*, 81 (2015) 148.
53. Z. Guo, G.S. Zhu, B. Gao, D.L. Zhang, G. Tian, Y. Chen, W.W. Zhang and S.L. Qiu, *Carbon*, 43 (2005) 2344.
54. C.Y. Li, S.Y. Wang, Z.H. Rong, X.Q. Wang, G.N. Gu and W.J. Sun, *J. Non–Cryst. Solids*, 356 (2010) 1246.
55. C. Vix–Guterl, E. Frazckowiak, K. Jurewicz, M. Friebe, J. Parmentier and F. Béguin, *Carbon*, 43 (2005) 1293.
56. J. Chmiola, G. Yushin, Y. Gogotsi, C. Portet, P. Simon and P.L. Taberna, *Science*, 313 (2006) 1760.
57. E. Raymundo–Piñero, K. Kierzek, J. Machnikowski and F. Béguin, *Carbon*, 44 (2006) 2498.
58. Q. Gao, L. Demarconnay, E. Raymundo–Piñero and F. Béguin, *Energy Environ Sci*, 5 (2015) 9611.
59. M.B. Wu, R.C. Li, X.J. He, H.B. Zhang, W.B. Sui and M.H. Tan, *New Carbon Mater*, 30 (2015) 86.
60. H.J. Zheng, A.M. Yu and C.A. Ma, *Russ. J. Electrochem*., 48 (2012) 1179.
61. A.Y. Rychagov, N.A. Urisson and Y.M. Vol'Fkovich, *Russ. J. Electrochem*., 37 (2001) 1172.
62. W.C. Chen, T.C. Wen and H. Teng, *Electrochim. Acta*, 48 (2003) 641.

63. Q.H. Huang, X.Y. Wang, J. Li, C.L. Dai, S. Gamboa and P.J. Sebastian, *J. Power Sources*, 164 (2007) 425.
64. I.H. Kim, J.H. Kim, B.W. Cho and K.B. Kim, *J. Electrochem. Soc*., 153 (2006) 1451.
65. B. Fang, Y.Z. Wei and M. Kumagai, *J. Power Sources*, 155 (2006) 487.
66. C.H. Kim, S.I. Pyun and H.C. Shin, *J. Electrochem. Soc*., 149 (2002) 93.
67. L. Wei, T. Shan and S. Yun, *Fuel*, 160 (2015) 35.
68. Y.R. Nian and H. Teng, *J. Electroanal. Chem*., 540 (2003) 119.